

Fault-Ride Through Performance Analysis of Grid Forming Inverter-Based Resources

ABSTRACT

Inverter-based resources (IBRs) have a different fault response than that of synchronous generators (SGs). To understand how the unique fault response of IBRs impacts the performance of protection system, it is vital to characterize the fault current of these sources. Such an understanding not only facilitates a more accurate modeling of IBRs in short circuit studies but also helps to design reliable protection schemes for IBR-dominated systems.

The fault response of IBRs primarily depends on their control system, which can be designed to meet different objectives. Existing grid codes and standards have mandated IBRs that are connected to the bulk power system to ride through various disturbances -- including short circuit faults -- and support the grid. Hence, various fault ride-through (FRT) strategies have been developed and incorporated in the IBR's control system. Current grid codes and standards provide certain general performance requirements for the FRT behavior of IBRs, and the details of the implementation are mostly left to the manufacturers, which often results in a proprietary and non-universal fault current signature for IBRs.

Unlike grid-following (GFL) IBRs, the fault response of grid-forming (GFM) IBRs have not been extensively investigated in the literature. GFM technology is an advanced control system designed to provide certain grid services, such as voltage and frequency support. These services are essential for maintaining stability of the power grid as more IBRs replace SGs.

This paper focuses on characterizing the fault response of GFM IBRs. It reviews existing FRT control strategies for GFM IBRs in the literature, and their fault current characteristic. A key part of the FRT control is the current limiting scheme, which ensures that the inverter current does not go beyond the maximum current limit and damages power electronic switches. The most common current limiting methods for GFM IBRs are discussed and compared. Moreover, the impact of different elements/parameters in the control system of GFM IBRs on the fault response of these sources is investigated through a detailed analysis and simulation study using generic electromagnetic transient based GFM models.

Keywords

Inverter-based resources (IBRs)
Grid-forming (GFM)
Fault response
Control system

INTRODUCTION

Over the past decade, there have been significant number of efforts that have analyzed the fault response of inverter-based resources (IBRs) [1]-[4]. The drive force behind these works have been the changing short circuit characteristic of the power system due to addition of more IBRs and the industry need to characterize the differences, model IBRs in fault analysis programs, and design protective relays that can ensure reliability of the protection system in grids with IBRs.

IBRs have a different fault current characteristic than that of synchronous generators (SGs). Fault current of IBRs depends mainly on their control system and is limited by the thermal threshold of power electronics switches. SG's fault current, on the other hand, is determined based on system physics and is normally significantly larger than that of IBRs. IBR's control system is usually designed to comply with the requirements of the host grid code or standard. Existing grid codes require IBRs to have the capability to ride through various disturbances, including short circuit faults, and support the grid. This is achieved through a specific scheme in the IBR's control system known as fault ride-through (FRT) strategy. Current grid codes and standards provide certain general performance requirements for the FRT strategy of IBRs, and the details of the implementation are mostly left to the manufacturers. The different and often proprietary implementations of FRT strategies lead to a non-universal fault current signature for IBRs. In summary, given the dependence of IBR fault current on the FRT control, characterizing the former requires an understanding of the latter.

The main focus of the existing literature on the fault response of IBRs is on grid-following (GFL) IBRs [1]-[4]. GFL refers to an IBR control technology whose primary objective is to regulate the active and reactive powers of the IBR with limited voltage and frequency support. During a fault, the FRT strategy of a GFL regulates the current at the inverter terminal such that certain control objectives are met. Typical objectives include limiting the sustained current passing through the power electronic switches (normally within 1.0-1.5 per unit), injecting positive-sequence reactive cur-

rent along with the negative sequence current, and prioritizing active or reactive currents [5], [6]. While the manufacturer-specific implementation of these requirements and corresponding FRT strategies may be different, the common denominator is that a GFL behaves as a voltage dependent current source during faults [2], [3]. Based on this understanding, commercial fault analysis programs model a GFL IBR with a current source whose current is a function of the terminal voltage and the FRT control [7]. In summary, the fault response of a GFL has been studied in the literature, and equivalent models have been developed by commercial fault analysis programs.

Despite the extensive work on the fault response of GFL IBRs, few works exist on the fault current characteristics of grid-forming (GFM) IBRs [20]. Hence, this paper reviews the existing literature on GFM FRT control and fault response characteristics. Similar to GFL, the fault current contribution of a GFM is controlled through fast switching of power electronics devices dependent upon manufacturer specific and often proprietary control scheme. However, given the differences in the control system of GFM and GFL IBRs, the fault response can be different. This paper reviews different GFM FRT strategies and current limiting methods namely, current saturation, virtual impedance, voltage limiter, and hybrid methods. The fault current signature of GFM with these methods is evaluated, and the key features are identified. Simulation case studies are presented to further demonstrate the findings.

GRID-FORMING IBR

A dominant share of present day IBRs use GFL control, which is shown to have challenges providing grid services in IBR-dominated grids. GFM is envisioned to be a potential solution, given its more advanced control capabilities [8]. GFM technology is an advanced control system designed to provide all or most of grid services, such as voltage and frequency support. GFM IBRs can provide certain grid services that cannot be offered to the same extent and robustness by GFL IBRs. This technology is expected to enhance the grid reliability when penetration of IBRs rises.

The recent trend in the industry tends to differentiate GFM IBRs from GFL IBRs based on their performance specifications and functional requirements. GFM performance requirements for operation within normal and abnormal grid conditions are documented in the literature [9]. Another approach to define GFM and GFL is based on control objectives. For a GFL IBR, in the first few cycles of a disturbance within the normal operating range of the voltage, the control system objective is normally to maintain a constant current phasor. For disturbances outside the normal operating range of the voltage, such as faults, the primary control objective is typically to regulate the current based on the specified FRT requirements and limit the magnitude of the sustained current to below the thermal threshold of power electronic switches. Changes in the current occur only during the transient time frame (tens of cycles) when the dynamics of the outer control loop, which regulates the active and reactive power, come into play. In the longer post-transient timeframe, GFL control may implement objectives such as maximum power point tracking, frequency response, and voltage regulation. On the other hand, GFM control system maintains a voltage phasor with a constant or nearly constant magnitude and phase angle in the sub-transient to transient time frame. During a fault, the objective is to uphold the desired voltage magnitude and phase angle and prioritize voltage or frequency support. Besides, by using a current limiting method, the control system ensures that the inverter current remains below the thermal limit of power electronic switches. The fault response of a GFM is determined based on its control objective, i.e., FRT strategy, in this condition. In the longer timescale, the control objective can be to adjust the terminal voltage and frequency to synchronize with other sources.

Note that more advanced and state-of-the-art GFL control systems are capable of providing voltage and frequency support in a timescale comparable to that of GFMs. Hence, the delineation between the definition of GFL and GFM

based on only the control objective may not be fully accurate.

GFM Control System

Figure 1 shows the typical control system of a GFM IBR in dq reference frame. This control system is comprised of two layers, namely the outer control loop and the inner control loops. The main objective of the outer control loop is to synchronize the GFM with the power grid and regulate the terminal voltage magnitude and angle. The most common configurations for the outer control loop are droop, virtual synchronous machine (VSM), dispatchable virtual oscillator (dVOC), and phase-locked loop (PLL). A reference voltage magnitude E_{ref} , phase angle θ_{ref} , and angular frequency ω_{ref} are generated by the outer control loop such that the reference active power P_{ref} , reactive power Q_{ref} , and voltage V_{ref} are followed at the inverter terminal. Moreover, ω_{ref} is used for abc to dq transformation of voltage and current measurements in the control system.

The second layer in the control system of a GFM IBR is where the inner control loops are implemented, namely the voltage and current control loops in Figure 1. E_{ref} from the outer control loop is fed to the voltage control loop as $V_{d,ref}^+$ so that the voltage magnitude at the inverter terminal becomes $E_{ref} \cdot V_{q,ref}^+$ is set to zero to align the dq axes of the control system with those of the grid voltage. The voltage control loop receives $V_{d,ref}^+$ and $V_{q,ref}^+$ voltage references and generates the desired setpoints of GFM terminal current (denoted by $I_{vd,ref}^+$ and $I_{vq,ref}^+$) such that the voltage at the inverter terminal follows $V_{d,ref}^+$ and $V_{q,ref}^+$. The reference currents $I_{vd,ref}^+$ and $I_{vq,ref}^+$ from the voltage control loop are then forwarded to the current control loop as $I_{d,ref}^+$ and $I_{q,ref}^+$ to be followed at the inverter terminal through voltage modulation signal v_{pwm} .

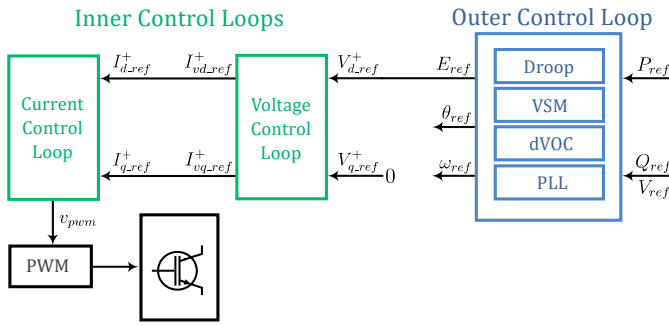


Figure 1. Typical control system of a GFM IBR.

FAULT RIDE-THROUGH STRATEGY OF GFM IBRS

During fault conditions, GFM control's attempt to maintain an internal voltage phasor may cause the desired current references $I_{vd_ref}^+$ and $I_{vq_ref}^+$ in Figure 1 to increase beyond the maximum current capacity of the inverter. To prevent this and to facilitate a successful FRT, control system of GFM IBRs is equipped with an FRT strategy, which includes additional control loops that are activated only during faults. An integral part of the FRT strategy is the current limiting method, which ensures that the actual setpoints of GFM current, $I_{d_ref}^+$ and $I_{q_ref}^+$ in Figure 1, remain below the maximum limit during faults. Other objectives, such as voltage or frequency support or compliance with the FRT requirements of the host grid code, can also be considered in designing the FRT strategy.

The fault response of a GFM IBR is largely dependent on its FRT strategy. Two general categories of FRT strategies for GFM IBRs exist in the literature:

1. Switching to GFL control structure upon detection of a fault, thus operating as a current source with a current limiting strategy [10].
2. Maintaining the GFM control structure during faults and employ a certain current limiting technique [11].

In the first category, the IBR control system is switched to GFL (which results in losing the voltage source behavior of GFM during a fault) via a fault detection algorithm. This method requires a backup PLL to synchronize the control system to the grid. Since the fault response under this FRT strategy is expected to be consistent with a GFL IBR which

is extensively studied in the literature, this FRT strategy has not been further reviewed in this paper.

The second strategy, on the other hand, keeps the GFM control structure, e.g., the control system of Figure 1, operational during FRT and uses a current limiting method to prevent overcurrent. The following sections detail the most common current limiting methods for GFM IBRs in the literature, including current saturation [11], [12], virtual impedance [13], [14], voltage limiter [15], [16], and hybrid [17], [18].

Current Saturation

Figure 2 illustrates the general overview of the GFM control system with the current saturation method. This current limiter is typically implemented between the voltage and current control loops, and the inverter current is limited by saturating the current references $I_{vd_ref}^+$ and $I_{vq_ref}^+$ generated by the voltage control loop. The saturated current references $I_{d_ref}^+$ and $I_{q_ref}^+$ are forwarded to the current control loop to be enforced at the inverter terminal. Depending on the reference frame of the control system, this method can be implemented in dq , abc , or $\alpha\beta$ frames.

Given that the current saturation method is implemented at the current control loop stage, its dynamic performance is tightly related to the dynamics of the current control loop. Since this loop has a higher bandwidth than the voltage control loop, current saturation is expected to limit the inverter current at a higher speed compared to other methods that are implemented at the voltage control loop stage, such as virtual impedance and voltage limiter.

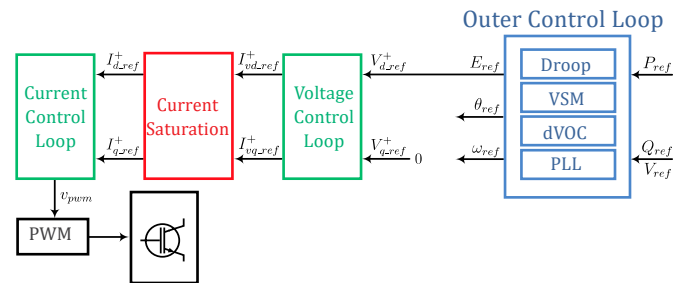


Figure 2. Control diagram of a GFM with current saturation method.

Virtual Impedance

Another common method in the literature for limiting the GFM inverter current during faults is virtual impedance. The idea in this method is to add a large virtual impedance between the inverter and the grid in the event of an overcurrent and so limit the inverter current. A general overview of this method is shown in Figure 3. As this figure illustrates, this method is implemented at the voltage control loop stage where the voltage drop across the virtual impedance is subtracted from the reference voltage E_{ref} of the outer control loop. As a result, the reference voltages $V_{d,ref}^+$ and $V_{q,ref}^+$ are reduced, thereby decreasing the effective voltage at the inverter terminal and so curtailing the current.

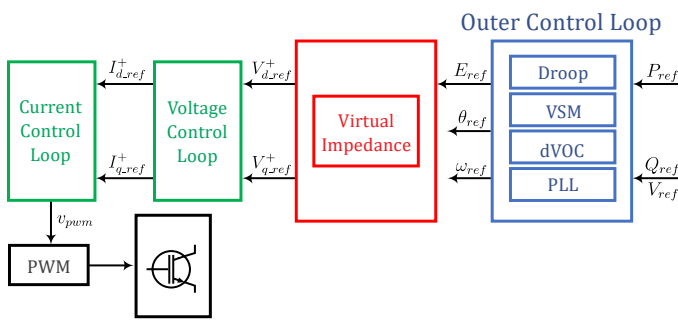


Figure 3. Control diagram of a GFM with virtual impedance method.

Unlike the current saturation method, the virtual impedance method does not override the voltage control loop, allowing voltage regulation during faults. However, due to the limited bandwidth of the voltage control loop, the virtual impedance method cannot limit the inverter current as fast as the current saturation method.

The magnitude and X/R ratio of the virtual impedance can be selected to be constant during FRT or adaptively change depending on system condition. Existing virtual impedance methods in the literature are typically designed to have a constant impedance and limit the inverter current to a constant threshold, i.e., the maximum current limit of power electronic switches. Although this can result in limiting the inverter current for symmetrical faults, it fails to achieve this objective for asymmetrical faults. Conversely, adaptive virtual impedance method can achieve current limitation during all types of faults [17]. However, it is important to appropriately select the magnitude and X/R of the virtual

impedance to achieve a reasonable and sufficient balance between stability, current limitation, and voltage support. A small X/R ratio, i.e., a more resistive virtual impedance, can result in a less oscillatory response with a lower possibility of overcurrent, but it can also make the GFM current mostly active, thereby potentially compromising voltage support during faults. Additionally, a virtual impedance with a large magnitude keeps the inverter current below the limit but may increase the risk of instability.

Voltage Limiter

This current limiting method directly reduces the voltage difference between the modulated voltage, v_{pwm} , and the terminal voltage, v_t , to a value lower than a certain threshold. A general overview of the GFM control system with this current limiter is shown in Figure 4. The implementation of the voltage limiter is usually achieved by modifying E_{ref} and θ_{ref} from the outer control loop to ensure that they are kept within a certain range such that $v_{ref} - v_t$ does not result in overcurrent. Similar to the virtual impedance method, voltage limiter is also implemented at the voltage control loop stage and is not able to limit the inverter current with a high speed. Consequently, temporary overcurrent may occur during the first few cycles of a fault.

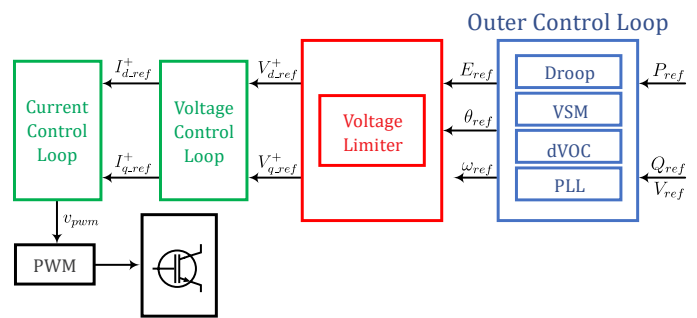


Figure 4. Control diagram of a GFM with voltage limiter method.

Hybrid

In this method, two or more of the above-mentioned current limiting methods are combined to achieve a superior performance and form a hybrid method. The general structure of a GFM control system with this method looks like Figure 5. An example of this method is to use current saturation during transients and virtual impedance for post-transients of a fault to ensure fast current limiting as well as voltage regulation during faults.

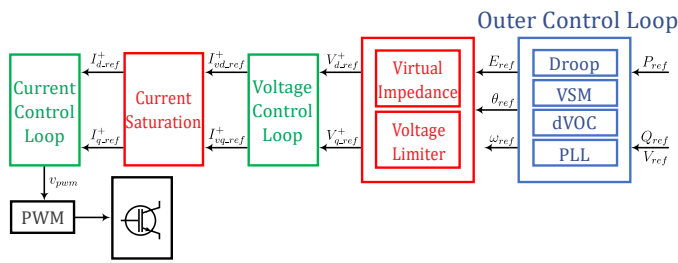


Figure 5. Control diagram of a GFM inverter with hybrid method.

FAULT CURRENT SIGNATURE OF GFM IBRs

This section analyzes fault current signature of GFM IBRs through simulation case studies. A generic electromagnetic transient (EMT) based model of a GFM, developed based on the latest FRT strategies in the literature and discussed above, is used. The details of the model can be found in [19]. The impact of different loops/logics in the control system of a GFM, including outer and inner control loops, current limiting method, negative-sequence current control loop, and frequency freezing function, on the fault response of GFM IBRs is investigated. The configuration of the IBR plant and the test system used in this study are shown in Figure 6 and Figure 7, respectively. The relevant parameters of these systems can be found in [19]. In all the simulation case studies of the paper, a bolted phase-B-to-phase-C-to-ground (BCG) fault is applied at $t = 5$ s at POM of the plant in Figure 7, and the measurements at POC of Figure 6, i.e., the inverter terminal, are examined.

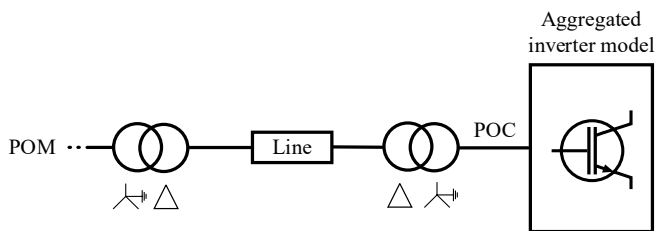


Figure 6. IBR plant configuration.

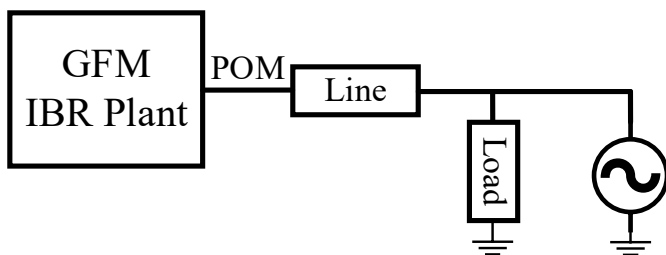


Figure 7. Test system.

Impact of Outer Control Loop

As mentioned in the last section, the outer control loop is responsible for power and voltage regulation as well as synchronizing the GFM control system with the grid. Different configurations can be used for the outer loop, such as droop, VSM, dVOC, etc. This section investigates how configuration of the outer control loop affects the fault current signature of GFM IBRs. The generic GFM model used in this study is equipped with droop and VSM in the outer control loop. Table 1 lists the default settings for the relevant parameters of droop and VSM.

Table 1. Parameters of the droop and VSM control loops.

PARAMETER	VALUE
Frequency droop gain (d_f)	5%
Voltage droop gain (d_v)	5%
VSM damping coefficient (D)	300
VSM inertia constant (H)	5 s

Droop vs VSM

This case compares the fault current of the GFM model when the outer control loop configuration is droop or VSM with the corresponding default parameters of Table 1. Figure 8 and Figure 9 show the measurements at POC during the fault when droop and VSM are used, respectively. In Figure 8(a) and Figure 9(a), the three-phase instantaneous currents are similar for both droop and VSM. Similarly, the magnitudes of the sequence currents are almost identical in Figure 8(b) and Figure 9(b). The angle of the negative-sequence current in Figure 8(c) and Figure 9(c) is also identical. However, the angle of the positive-sequence current is different between droop and VSM. Moreover, this angle varies throughout the fault when droop is used, while it is almost constant for VSM. The larger variation of $\angle I^+$ for droop is due to deviation of the IBR control system frequency, ω_{ref} from the rated value. This causes the control system to lose synchronism with the grid. The larger resistance-to-change-of-frequency behavior that VSM presents makes the frequency deviation smaller in this configuration compared to droop, which keeps the positive-sequence current angle more stable. To illustrate this point further, Figure 10 depicts ω_{ref} for droop and VSM in this case. It can be seen that ω_{ref} remains much closer to the rated value of 1 pu in VSM compared to droop. Therefore, this case shows that chang-

ing configuration of the outer control loop from droop to VSM impacts only the angle of the positive-sequence current. Similar results were found for other fault types, locations, and resistances as well. It is important to highlight that parameterization of the droop and VSM can play a major role in the fault response characteristics of GFM

IBRs. In this study, the parameters of Table 1 are selected such that a fast load sharing is achieved by the droop, and a resistance to rate of change of the frequency behavior is presented by VSM. The parameters of droop and VSM can be selected such that they become equivalent, which will make their fault current characteristic identical.

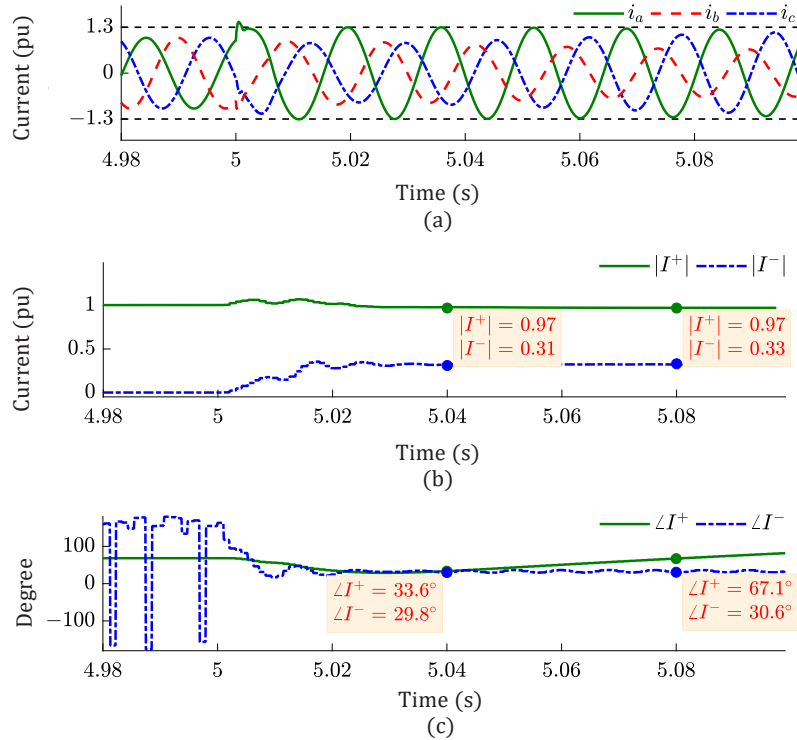


Figure 8. Measurements for droop. (a) Instantaneous currents. (b) Magnitude of the sequence currents. (c) Angle of the sequence currents.

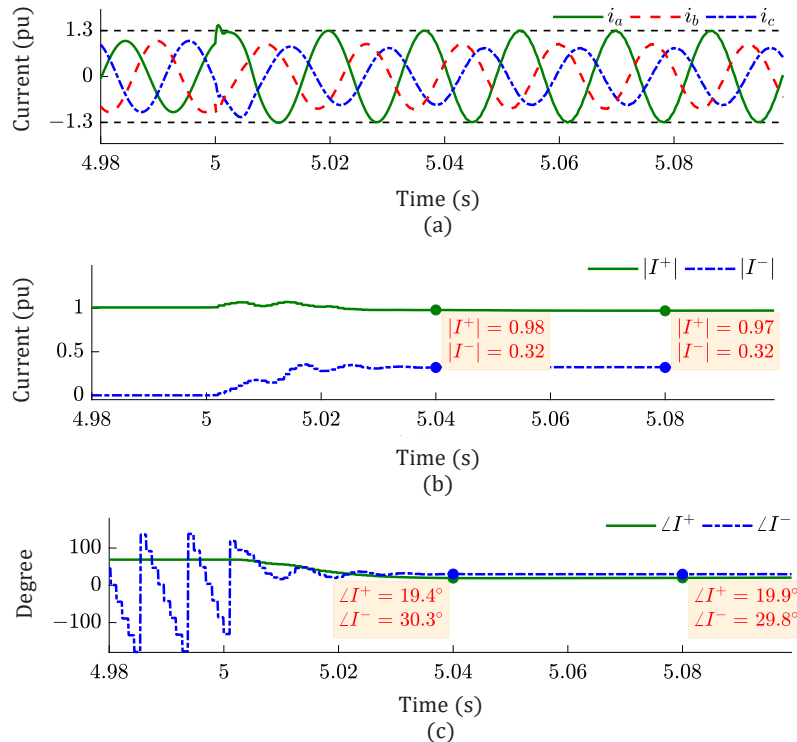


Figure 9. Measurements for VSM. (a) Instantaneous currents. (b) Magnitude of the sequence currents. (c) Angle of the sequence currents.

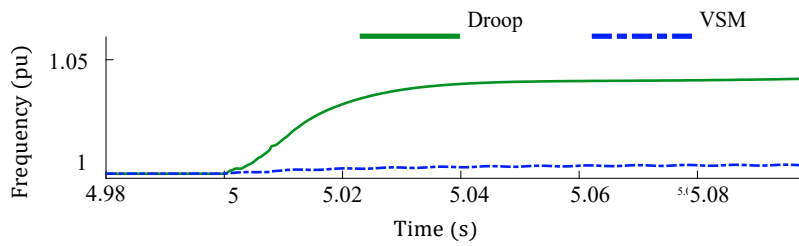


Figure 10. The reference angular frequency of the IBR’s control system for droop and VSM.

Droop Parameters

This case evaluates how variation of droop parameters, including frequency droop, d_f , and voltage droop, d_v , gains, impact the fault current of GFM IBRs. As mentioned above, only the angle of the positive-sequence current is impacted by the outer control loop, so the following studies the impact of d_f and d_v on this quantity only.

First, the response of the GFM model is analyzed for different frequency droop gains in the active power-frequency droop loop, including 1% and 5%, while d_v remains constant at the default value in Table 1. Figure 11 shows the

angle of the positive-sequence current during the fault for the two values of d_f . This figure demonstrates that $\angle I^+$ is highly impacted by d_f . Variation of $\angle I^+$ throughout the fault becomes more drastic as d_f increases. The reason behind this is that a larger d_f results in a more extreme deviation of ω_{ref} from 1 pu, thereby intensifying variations of $\angle I^+$ during the fault (similar to the previous case). Figure 12 displays ω_{ref} for different values of d_f in this case. It can be observed that ω_{ref} deviates from 1 pu more significantly for a larger d_f . Therefore, this case shows that increasing d_f makes $\angle I^+$ to change more drastically during the fault.

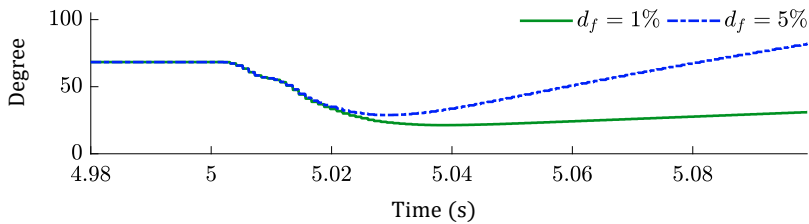


Figure 11. Angle of the positive-sequence current for different frequency droop gains.

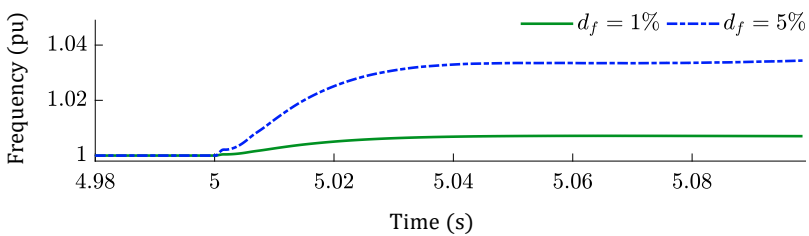


Figure 12. The reference angular frequency of the IBR control system for different frequency droop gains.

Secondly, the effect of the voltage droop gain, d_v , on the fault current signature of GFM IBRs is investigated. The reactive power-voltage control loop is the same in droop and VSM, so the results obtained in this case are applicable to both configurations. The fault response of the GFM model for two values of d_v , including 1% and 10%, is examined, while d_f has the default value. Figure 13 illustrates $\angle I^+$ during the fault. This figure shows that $\angle I^+$ is not impacted by d_v because the reactive power-voltage control loop impacts

the voltage magnitude at the inverter terminal, and the voltage angle, which determines $\angle I^+$, is regulated by the active power-frequency control loop. Interestingly, the magnitude of I^+ is also not impacted by d_v in this case. The reason is that the GFM model uses a current limiter technique that maximizes the inverter current during faults and keeps the voltage magnitude constant for the same fault condition irrespective of the outer control loop parameters.

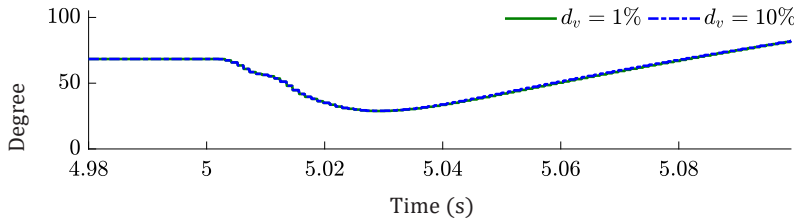


Figure 13. Angle of the positive-sequence current for different voltage droop gains.

VSM Parameters

The effect of VSM parameters, including inertia constant, H , and damping coefficient, D , on the fault response of GFM IBRs is examined. Firstly, the angle of the positive-sequence current is evaluated for different values of H , and then the analysis is repeated by changing D .

Figure 14 depicts $\angle I^+$ for H equal to 0.05 s and 5 s, while D is set to the default value in Table 1. It is demonstrated that $\angle I^+$ does not change much as H changes. As discussed earlier, the damped inertia-based characteristic of VSM maintains ω_{ref} much closer to the rated value compared to droop. Therefore, the angle of the positive-sequence current is not impacted by the value of H . It is important

to note that the damping coefficient of $D = 300$ in this case also contributes to limiting the deviation of ω_{ref} . If D is smaller, variations of H can potentially impact $\angle I^+$.

The impact of the VSM damping coefficient on the fault current signature of GFM IBRs is also evaluated. The fault response of the GFM model is captured for D equal to 150 and 600 with $H = 5$ s. The obtained results are demonstrated in Figure 15. Similar to H , varying D also does not impact the angle of the IBR's positive-sequence current much as well as GFM's fault current signature. The underlying reason for this behavior is the non-significant deviation of ω_{ref} from 1 pu with VSM, like the previous case.

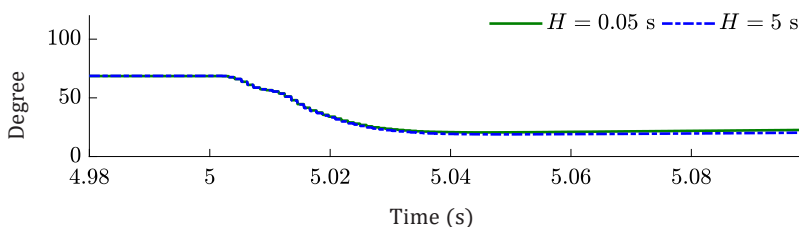


Figure 14. Angle of the positive-sequence current for different inertia constants.

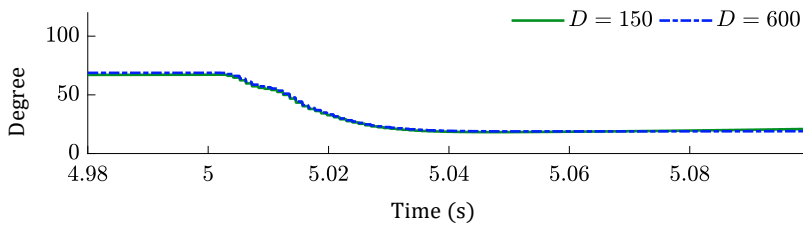


Figure 15. Angle of the positive-sequence current for different damping coefficients.

Impact of Frequency Freezing During FRT

To avoid deviation of the reference angular frequency of the IBR control system, ω_{ref} in Figure 5, from the rated value during FRT, which can result in transient instability, it has been proposed that the GFM control system freezes ω_{ref} during faults [17]. This section investigates the impact of this practice on the fault response of GFM IBRs.

Consider the same fault condition as in the previous cases when ω_{ref} is frozen during the fault. Figure 16 displays the fault response of the GFM model for droop and VSM. This figure shows that the magnitude and angle of the sequence

currents precisely match each other for both the droop and VSM. Freezing the frequency overrides the active power-frequency control loop of droop and VSM. As a result, since the reactive power-voltage control loop is identical in droop and VSM, their fault response becomes identical. Therefore, the IBR's fault current signature becomes independent of the active power-frequency control loop parameters if the frequency is frozen during FRT. Although freezing the frequency can enhance transient stability of the IBR control system, it can hinder a smooth fault recovery, especially when the system frequency or voltage angle after the fault clearance is different from the pre-fault values.

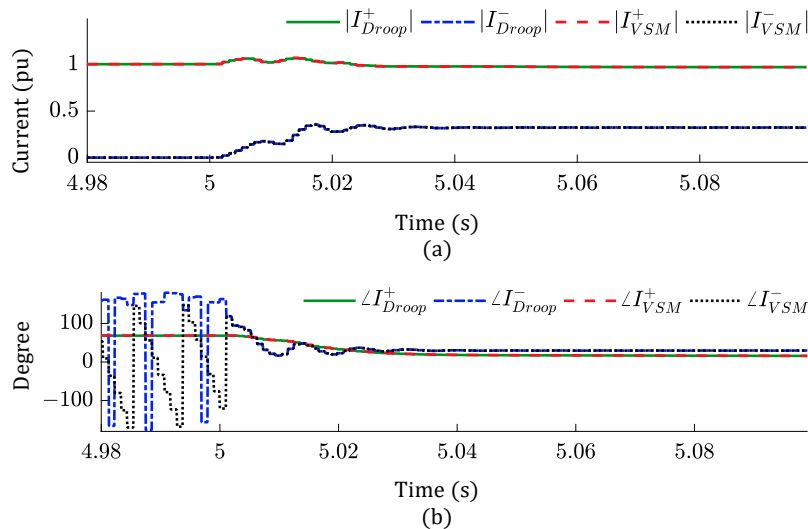


Figure 16. Measurement for droop and VSM. (a) Magnitude of the sequence currents. (b) Angle of the sequence currents.

Impact of Current Limiting Method

This section investigates the impact of different current limiting methods on the fault current signature of GFM IBRs. Virtual impedance, current saturation, and hybrid methods are considered in the analysis.

Virtual Impedance

As discussed earlier, one of the most common methods in the literature to limit the current of GFM IBRs during FRT is the virtual impedance method. In this method, the inverter current is limited by adding a large virtual impedance in the fault path. The GFM model used in this study is equipped with an adaptive virtual impedance with a configurable X/R ratio that maximizes the positive-sequence current magnitude during FRT.

Figure 17 shows the measurements during the fault when the IBR uses the virtual impedance method with an X/R

ratio equal to 2, and the frequency is frozen. As depicted in Figure 17(a), the instantaneous phase currents are limited below the 1.3 pu limit of the inverter slowly because the virtual impedance method acts upon the references of the voltage control loop, which has a low bandwidth. Consequently, the inverter experiences a temporary overcurrent during the fault. Figure 17(b) shows the magnitude of the positive- and negative-sequence currents. Since the virtual impedance method is applied on the positive-sequence current, $|I^+|$ settles slower than $|I^-|$, which is limited by current saturation method in the negative-sequence current control loop. The speed of the virtual impedance method can be enhanced by tuning the parameters of the controllers in the voltage control loop, but a compromise exists between speed and stability of this method that does not allow a noticeable reduction of the time constant.

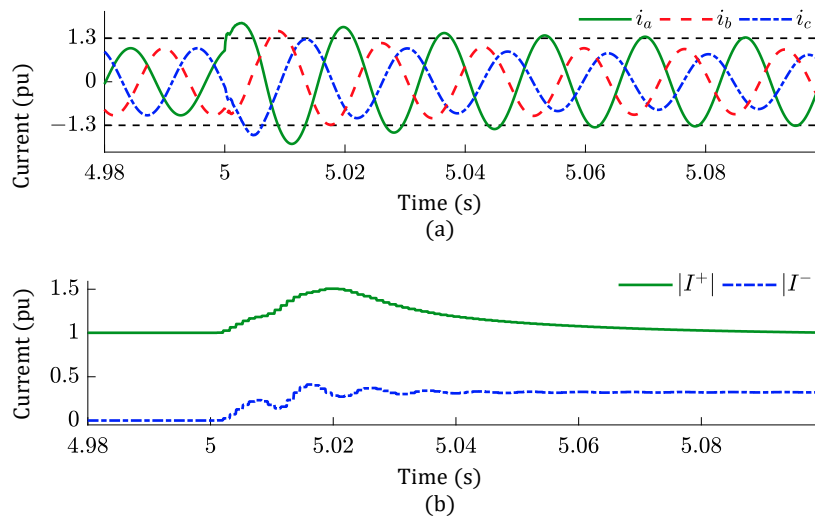


Figure 17. Measurements when the IBR uses virtual impedance method. (a) Instantaneous currents. (b) Magnitude of the sequence currents.

The amount of active and reactive currents generated by an IBR during FRT is of great importance, as it impacts the level of voltage and frequency support, protection system performance, etc. Hence, Figure 18 demonstrates the active and reactive components of the positive- and negative-sequence currents injected by the GFM model in this case. r and p subscripts in this figure denote the reactive and active components, respectively. When the virtual impedance method is used, the ratio of I_r^+ to I_p^+ is directly impacted by the X/R of the virtual impedance. A larger X/R ratio makes

the IBR's positive-sequence current more reactive. For example, in this case with $X/R = 2$, Figure 18(a) shows that I_r^+ ramps up as soon as the fault begins, while I_p^+ drops. If the fault is resistive, the fault resistance will be added in series to the virtual impedance, which can increase I_p^+ . Hence, I_r^+ to I_p^+ ratio is primarily determined by the X/R ratio of the virtual impedance, fault resistance and fault location. The active and reactive components of the negative-sequence current are also shown in Figure 18(b). Since the negative-sequence current is regulated based on the K-factor control,

I_p^- is always zero, and I_r^- is negative, meaning that the IBR is consuming negative-sequence reactive current. The value of I_r^- depends on the K-factor and the magnitude of the negative-sequence voltage and is not affected by the current limiting method of the positive-sequence current.

X/R ratio: To get a better understanding of how I_r^+ to I_p^+ ratio is affected by the X/R of the virtual impedance, the fault response of the model was assessed for different values of X/R, including 0 and 6. Figure 19 depicts I_r^+ and I_p^+ of the IBR in this case. When X/R = 0, i.e., a purely resistive virtual impedance, the positive-sequence current is highly

active in Figure 19(a) with I_p^+ being almost equal to the pre-fault value of 1 pu. Although the virtual impedance is purely resistive in this case, I_r^+ is not zero in Figure 19(a) due to the collector system reactances, such as those of the step-up transformers. Figure 19(b) shows that increasing X/R ratio increases I_r^+ and decreases I_p^+ significantly compared to Figure 19(a). As a result, this case demonstrates that the X/R ratio of the virtual impedance directly impacts the level of active and reactive currents generated by the IBR during faults.

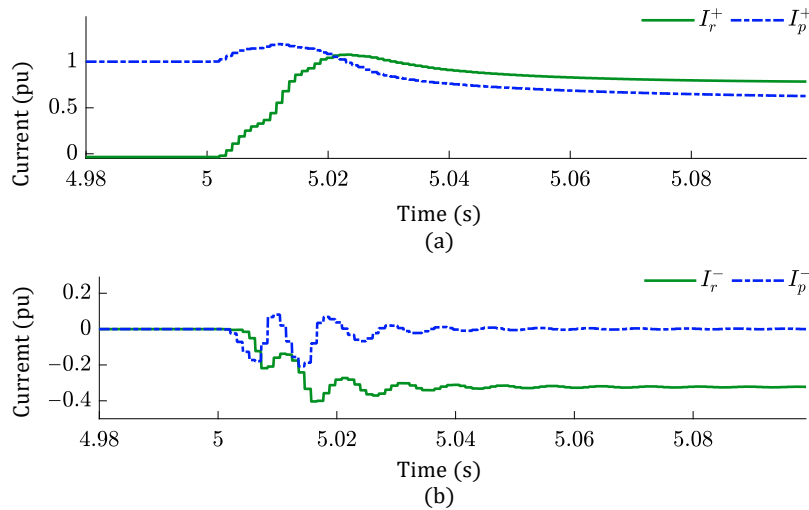


Figure 18. Measurements when the IBR uses virtual impedance method. (a) Positive-sequence active and reactive currents. (b) Negative-sequence active and reactive currents.

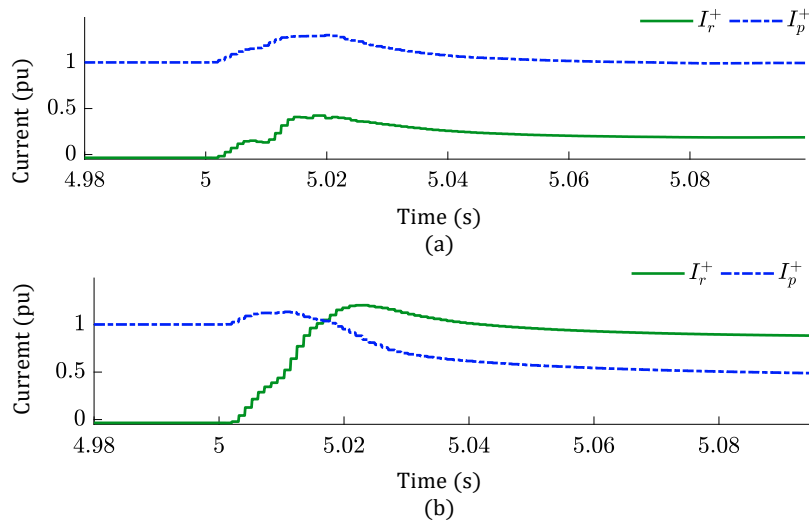


Figure 19. Measurements of positive-sequence active and reactive currents when the IBR uses virtual impedance method. (a) X/R= 0. (b) X/R= 6.

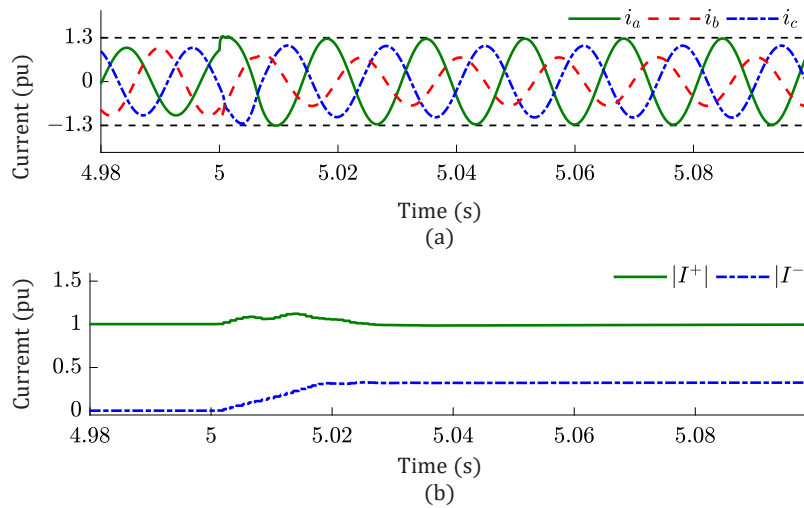


Figure 20. Measurements when the IBR uses current saturation. (a) Instantaneous currents. (b) Magnitude of the sequence currents.

Current Saturation

Another common method in the literature for limiting the current of GFM IBRs during FRT is current saturation. As explained earlier, in this method, the overcurrent is prevented by saturating the references of the current control loop. Figure 20 shows the fault response of the GFM model when current saturation method is employed. The instantaneous phase currents in Figure 20(a) are limited below 1.3 pu faster than Figure 17(a) with virtual impedance method. The high bandwidth of the inner current control loop allows high speed tracking of the saturated current references with minimum over/undershoot, thereby facilitating a quicker current limiting than the virtual impedance method, which is applied at the voltage control loop stage. The settling time of the positive-sequence current magnitude has also decreased significantly in Figure 20(b) compared to Figure 17(b) with virtual impedance method.

Figure 21 displays the active and reactive components of the sequence currents in this case. Although the fault is bolted and close-in, the positive-sequence current of the IBR is highly active because there is no mechanism in the current saturation method to increase reactive current proportional to the voltage drop during faults (unlike the virtual impedance method). This results in a noticeable reduction of the voltage support provided by the IBR during this fault compared to previous case with virtual impedance method in Figure 18(a). Unlike the virtual impedance method, there is no mechanism or settable parameter (like the X/R ratio) in the current saturation method that can facilitate regulation of the positive-sequence active and reactive currents during FRT. In the negative-sequence circuit, however, the K-factor control ensures generation of a purely reactive current irrespective of the current limiting method used in the positive-sequence circuit similar to the previous case.

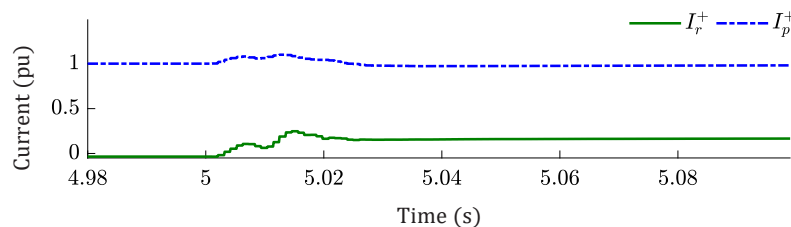


Figure 21. Positive-sequence active and reactive currents when the IBR uses current saturation.

Hybrid Method

The fault response of GFM IBRs is analyzed when the hybrid current limiting method is used. In the GFM model, the hybrid method uses current saturation for the first two cycles of the fault and then switches to the virtual impedance for the rest of the fault. Further details about implementation of this method can be found in [19].

Figure 22 and Figure 23 show the fault response of the GFM model when the hybrid method with an X/R ratio of 2 is used, and the frequency freezing function is enabled. Figure 22(a) shows a significant improvement in high-speed limiting of the phase currents below the 1.3-pu limit compared to Figure 17(a) with virtual impedance method. Current limiting capability of the hybrid method is close to that of current saturation in Figure 20(a).

Figure 22(b) demonstrates that the final values of $|I^+|$ and $|I^-|$ are close to those measured for the virtual impedance and current saturation methods, verifying that the magnitudes of the sequence currents are not impacted by the current limiting strategy. The settling time of $|I^+|$ is also close to current saturation case. Given that the hybrid method uses virtual impedance for the post-transient period of the fault, the final values of I_r^+ and I_p^+ in Figure 23 are close to those in Figure 18(a) for the virtual impedance with the same X/R ratio. Thus, this case shows that the hybrid method has the benefits of both virtual impedance and current saturation techniques. Not only can it limit the inverter current with a high speed, like the current saturation method, but it can also regulate active and reactive currents of the IBR, similar to the virtual impedance method.

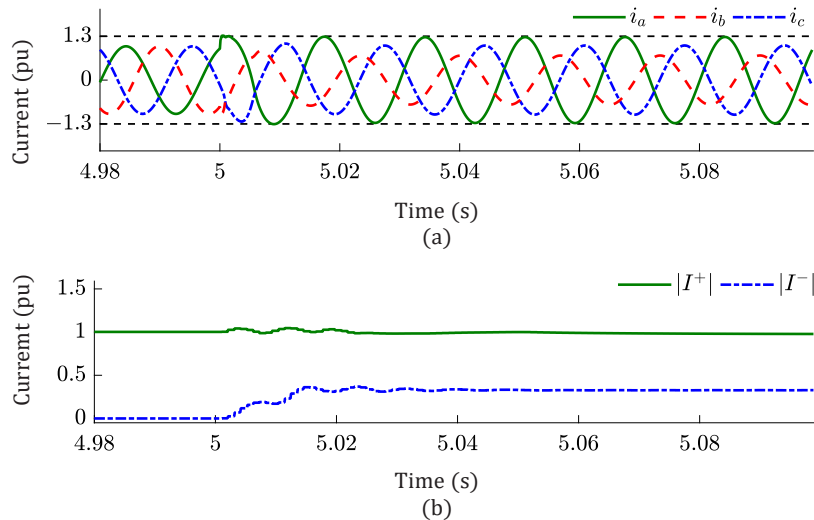


Figure 22. Measurements when the IBR uses the hybrid method. (a) Instantaneous currents. (b) Magnitude of the sequence currents.

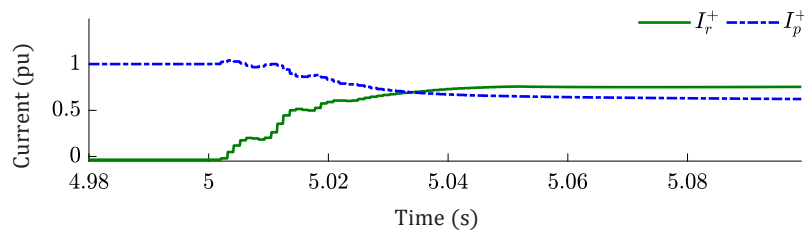


Figure 23. Positive-sequence active and reactive currents when the IBR uses the hybrid method.

Table 2 summarizes the above analyses on the performance of different current limiting methods from current limitation performance and fault current controllability perspectives.

Table 2. Performance comparison of different current limiting methods for GFM IBRs.

CURRENT LIMITING METHOD	CURRENT LIMITATION PERFORMANCE	FAULT CURRENT CONTROLLABILITY
Virtual impedance	<ul style="list-style-type: none"> • Slow current limiting • Temporary overcurrent during transients • Effective during steady state of a fault 	<ul style="list-style-type: none"> • Active and reactive currents can be regulated using X/R ratio of virtual impedance
Current saturation	<ul style="list-style-type: none"> • Fast current limiting • Effective during transients and steady state of a fault 	<ul style="list-style-type: none"> • Active and reactive currents cannot be regulated • No mechanism to increase reactive current proportional to voltage drop
Hybrid	<ul style="list-style-type: none"> • Potentially fast current limiting • Potentially effective during transients and steady state of a fault 	<ul style="list-style-type: none"> • Depends on the type of the combined current limiters

Impact of Negative-Sequence Current Control Strategy

The negative-sequence current of an IBR plays an important role in its fault current signature and directly impacts the performance of the protection system in the vicinity of IBRs. In this paper, two implementations of the negative-sequence current control strategy in GFM IBRs are analyzed, including K-factor and voltage imbalance removal controls. In the K-factor control method, the IBR generates a purely reactive negative-sequence current proportional to the magnitude of the negative-sequence voltage and a scalar K. The objective in the voltage imbalance removal method, however, is to inject a negative-sequence current that can suppress the voltage imbalance in the system, i.e., the negative-sequence voltage. Previous sections of the paper presented several case studies when the K-factor control is enabled, and it was demonstrated that with this strategy, the IBR consumes a reactive negative-sequence current. Hence, the following focuses on the voltage imbalance removal strategy.

Figure 24 demonstrates the fault response of the GFM model with the voltage imbalance removal strategy. As Figure 24(a) shows, $|I^+|$ and $|I^-|$ are the same as the ones in the previous cases, showing that the allocated capacity

to the sequence currents is not impacted by the current limiting method or the positive- and negative-sequence control loops and is determined such that the phase currents are maximized. Moreover, Figure 24(b) shows that the IBR presents a totally different behavior compared to the previous cases with K-factor control, e.g., in Figure 18(b). The attempt of the control system to suppress the negative-sequence voltage results in consumption of a large negative-sequence active current by the IBR in Figure 24(b), making the negative-sequence reactive current almost zero. Such a combination of I_p^- and I_r^- might not be desirable because it does not conform with the corresponding requirements of IEEE Std. 2800-2022 [5], which mandates IBRs to inject an almost purely reactive negative-sequence current during faults.

Impact of Inner Current Control Loop

The impact of the inner current control loop of the GFM IBRs on the fault current of these sources is similar to GFL IBRs, already investigated in the literature. The primary effect is on the current transients, especially the peak of the current, during the first few cycles of the fault. The gains of the PI controllers in this loop affect the speed at which the current references are followed.

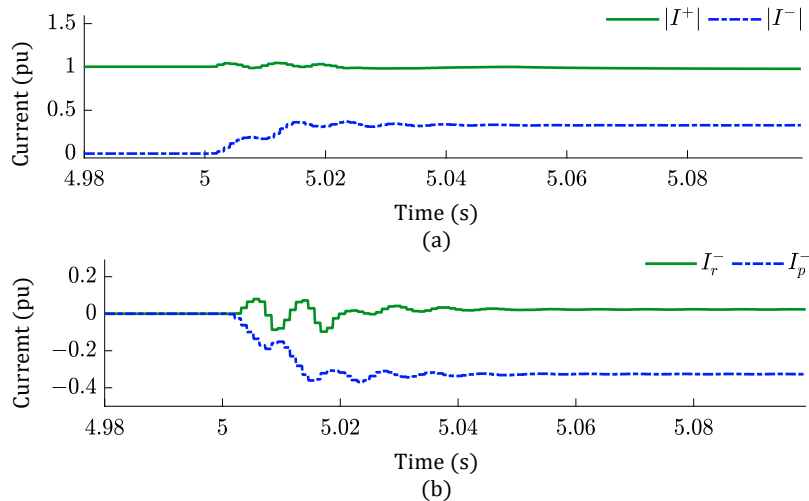


Figure 24. Measurements when the IBR uses the voltage imbalance removal strategy. (a) Magnitude of the sequence currents. (b) Negative-sequence active and reactive currents.

SUMMARY

This paper investigated the fault response of GFM IBRs. An introduction on definition of GFM IBRs and their control system was presented. The paper reviewed the existing FRT strategies for GFM IBRs in the literature. Control structure for various FRT strategies with different current limiting methods, including current saturation, virtual impedance, voltage limiter, and hybrid, was discussed. Furthermore, the impact of different loops in the control system of GFM IBRs on the fault current signature of these sources was evaluated. The analysis was accompanied by EMT-based simulations using generic GFM IBR models.

REFERENCES

- [1] Joint Working Group of Transmission & Distribution Committee, Electric Machinery Committee, Power System Relaying Committee, “Fault Current Contributions from Wind Plants,” IEEE PES Technical Report PES-TR26, Jan. 2013.
- [2] *Short-Circuit Phasor Models of Converter-Based Renewable Energy Resources for Fault Studies*. EPRI, Palo Alto, CA: 2017. 3002010936.
- [3] T. Kauffmann et al, “An Accurate Type III Wind Turbine Generator Short Circuit Model for Protection Applications,” *IEEE Trans. Power Del.*, vol. 32, no. 6, pp. 2370–2379, Dec. 2017.
- [4] IEEE/NERC Task Force on Short-Circuit and System Performance Impact of Inverter Based Generation, “Impact of Inverter Based Generation on Bulk Power System Dynamics and Short Circuit Performance,” IEEE PES Technical Report PES-TR68, Jul. 2018.
- [5] IEEE Std 2800-2022 – IEEE Standard for Interconnection and Interoperability of Inverter-Based Resources (IBR) Interconnecting with Associated Transmission Electric Power Systems. Apr. 2022. <https://standards.ieee.org/project/2800.html>.
- [6] FNN, VDE. “VDE-AR-N 4120: Technische Regeln für den Anschluss von Kundenanlagen an das Hochspannungsnetz und deren Betrieb (TAR Hochspannung).” VDE-Verlag, Berlin (2018).
- [7] Power System Relaying Committee Working Group C24, Modification of Commercial Fault Calculation Programs for Wind Turbine Generators, IEEE PES Technical Report PES-TR78, Jun. 2020.
- [8] NERC, “Grid forming technology: Bulk power system reliability considerations,” tech. rep., North American Electric Reliability Corporation (NERC), Atlanta, GA, USA, 2021.
- [9] B. Kroposki et. al, “UNIFI Specifications for Grid-forming Inverter-based Resources - Version 1,” Universal Interoperability for Grid-Forming Inverters (UNIFI), UNIFI-2022-2-1, Dec. 2022.
- [10] L. Zhang, L. Harnefors, and H.-P. Nee, “Power-synchronization control of grid-connected voltage-source converters,” *IEEE Trans. Power Syst.*, vol. 25, no. 2, pp. 809–820, May 2010.
- [11] R. Rosso, S. Engelken, and M. Liserre, “On the implementation of an FRT strategy for grid-forming converters under symmetrical and asymmetrical grid faults,” *IEEE Trans. Ind. Appl.*, vol. 57, pp. 4385–4397, Sept. 2021.

- [12] B. Fan, T. Liu, F. Zhao, H. Wu and X. Wang, "A Review of Current-Limiting Control of Grid-Forming Inverters Under Symmetrical Disturbances," in *IEEE Open Journal of Power Electronics*, vol. 3, pp. 955-969, 2022.
- [13] M. Eggers, P. Teske and S. Dieckerhoff, "Virtual-Impedance-Based Current-Limitation of Grid-Forming Converters for Balanced and Unbalanced Voltage Sags," 2022 IEEE 13th International Symposium on Power Electronics for Distributed Generation Systems (PEDG), Kiel, Germany, 2022, pp. 1-6, <https://doi.org/10.1109/PEDG54999.2022.9923159>.
- [14] P. Piya, M. Ebrahimi, M. Karimi-Ghartemani, and S. A. Khajehoddin, "Fault ride-through capability of voltage-controlled inverters," *IEEE Trans. Ind. Electron.*, vol. 65, pp. 7933–7943, Oct. 2018.
- [15] J. Erdocia, A. Urtasun, and L. Marroyo, "Dual voltage-current control to provide grid-forming inverters with current limiting capability," *IEEE J. Emerg. Sel. Topics Power Electron.*, vol. 10, no. 4, pp. 3950–3962, Aug. 2022.
- [16] J. M. Bloemink and M. R. Iravani, "Control of a multiple source microgrid with built-in islanding detection and current limiting," *IEEE Trans. Power Del.*, vol. 27, no. 4, pp. 2122–2132, Oct. 2012.
- [17] M. -A. Nasr and A. Hooshyar, "Controlling Grid-Forming Inverters to Meet the Negative-Sequence Current Requirements of the IEEE Standard 2800-2022," in *IEEE Trans. on Power Del.*, vol. 38, no. 4, pp. 2541-2555, Aug. 2023.
- [18] S. F. Zarei, H. Mokhtari, M. A. Ghasemi, and F. Blaabjerg, "Reinforcing fault ride through capability of grid forming voltage source converters using an enhanced voltage control scheme," *IEEE Trans. Power Del.*, vol. 34, pp. 1827–1842, Oct. 2019.
- [19] *Investigating the Fault Response of Grid Forming Inverter-Based Resources*. EPRI, Palo Alto, CA: 2023. [3002027139](https://doi.org/10.21203/rs.3.rs-3002027/v1).
- [20] U. Muenz, S. Bhela, N. Xue, A. Banerjee, M. J. Reno, D. Kelly, E. Farantatos, A. Haddadi, D. Ramasubramanian, and A. Banaie, "Protection of 100% Inverter-dominated Power Systems with Grid-Forming Inverters and Protection Relays – Gap Analysis and Expert Interviews," Sandia National Laboratories, SAND204-04848, 2024.

DISCLAIMER OF WARRANTIES AND LIMITATION OF LIABILITIES

THIS DOCUMENT WAS PREPARED BY THE ORGANIZATION(S) NAMED BELOW AS AN ACCOUNT OF WORK SPONSORED OR COSPONSORED BY THE ELECTRIC POWER RESEARCH INSTITUTE, INC. (EPRI). NEITHER EPRI, ANY MEMBER OF EPRI, ANY COSPONSOR, THE ORGANIZATION(S) BELOW, NOR ANY PERSON ACTING ON BEHALF OF ANY OF THEM:

(A) MAKES ANY WARRANTY OR REPRESENTATION WHATSOEVER, EXPRESS OR IMPLIED, (I) WITH RESPECT TO THE USE OF ANY INFORMATION, APPARATUS, METHOD, PROCESS, OR SIMILAR ITEM DISCLOSED IN THIS DOCUMENT, INCLUDING MERCHANTABILITY AND FITNESS FOR A PARTICULAR PURPOSE, OR (II) THAT SUCH USE DOES NOT INFRINGE ON OR INTERFERE WITH PRIVATELY OWNED RIGHTS, INCLUDING ANY PARTY'S INTELLECTUAL PROPERTY, OR (III) THAT THIS DOCUMENT IS SUITABLE TO ANY PARTICULAR USER'S CIRCUMSTANCE; OR

(B) ASSUMES RESPONSIBILITY FOR ANY DAMAGES OR OTHER LIABILITY WHATSOEVER (INCLUDING ANY CONSEQUENTIAL DAMAGES, EVEN IF EPRI OR ANY EPRI REPRESENTATIVE HAS BEEN ADVISED OF THE POSSIBILITY OF SUCH DAMAGES) RESULTING FROM YOUR SELECTION OR USE OF THIS DOCUMENT OR ANY INFORMATION, APPARATUS, METHOD, PROCESS, OR SIMILAR ITEM DISCLOSED IN THIS DOCUMENT.

REFERENCE HEREIN TO ANY SPECIFIC COMMERCIAL PRODUCT, PROCESS, OR SERVICE BY ITS TRADE NAME, TRADEMARK, MANUFACTURER, OR OTHERWISE, DOES NOT NECESSARILY CONSTITUTE OR IMPLY ITS ENDORSEMENT, RECOMMENDATION, OR FAVORING BY EPRI.

EPRI PREPARED THIS REPORT.

The information, data, or work presented herein was funded in part by the Advanced Research Projects Agency-Energy (ARPA-E), U.S. Department of Energy, under Award Number DE-AR0001570, and in part by the UNIFI Consortium from the Alliance for Sustainable Energy, LLC, Managing and Operating Contractor for the National Renewable Energy Laboratory for the U.S. Department of Energy. The views and opinions of authors expressed herein do not necessarily state or reflect those of the United States Government or any agency thereof.

About EPRI

Founded in 1972, EPRI is the world's preeminent independent, non-profit energy research and development organization, with offices around the world. EPRI's trusted experts collaborate with more than 450 companies in 45 countries, driving innovation to ensure the public has clean, safe, reliable, affordable, and equitable access to electricity across the globe. Together, we are shaping the future of energy.

EPRI CONTACTS

EVANGELOS FARANTATOS, *Sr. Principal Team Lead*
650.855.2214, efarantatos@epri.com

AMIN BANAIE, *Engineer IV*
302.417.0131, abanaie@epri.com

ABOUTALEB HADDADI, *Technical Leader II*
865.218.8015, ahaddadi@epri.com

DEEPAK RAMASUBRAMANIAN, *Technical Leader II*
865.218.8178, dramasubramanian@epri.com

For more information, contact:

EPRI Customer Assistance Center
800.313.3774 • askepri@epri.com



3002029578

April 2024

EPRI

3420 Hillview Avenue, Palo Alto, California 94304-1338 USA • 650.855.2121 • www.epri.com

© 2024 Electric Power Research Institute (EPRI), Inc. All rights reserved. Electric Power Research Institute, EPRI, and TOGETHER...SHAPING THE FUTURE OF ENERGY are registered marks of the Electric Power Research Institute, Inc. in the U.S. and worldwide.